Self-actuated Piezoresistive Cantilever based AFM for Single Ion Implantation

A. Schuh, Y. Sarov, Tzv. Ivanov and I. W. Rangelow
Ilmenau University of Technology, Department of Micro- und Nanoelectronic Systems, Institute of Micro- and Nanoelectronics, Faculty of Electrical Engineering and Information Technology, Postfach 100565, 98684 Ilmenau, Germany

C. D. Weis, A. Batra, A. Persaud and T. Schenkel
Lawrence Berkeley National Laboratory, 1 Cyclotron Road, Berkeley, California 94114

Abstract

Quantum computing devices realized in silicon based solid states require precise spatial placement of single donors within the target. Ion impacts can be detected by different effects, like ion beam induced current changes in FET channels. Here, an ion impact detection system with automatic ion beam control and alignment of the FET channel with small collimating holes drilled into the cantilever of an AFM is reported. This is possible with a LabVIEW based IBIC detection program. The detection system is applied on induced current changes due to the exposure to a pulsed 48 keV Xe^{6+} ion beam. By scanning the AFM cantilever in a small distance above the surface of the FET, low energy 20 and 36 keV $Ar^{2+,3+}$ ions can be implanted into cells within a predefined array. A response during mapping is visible, when the holes in the cantilever are aligned to the channel of the transistor.

Index Terms - Quantum Computing, single ion implantation, AFM, IBIC

I. INTRODUCTION

The aggressive miniaturization of transistors permanently requires new technologies. According to Moor's law, transistor channels will be only a few nanometers in width in the near future. Homogenous, controlled placement of donors in modern conventional Field Effect Transistors (FET) is proposed to be a large benefit in terms of less fluctuating threshold voltages [1, 2].
Also, in silicon based solid state quantum computing a precise spatial placement of donors is essential for the development of such devices, since the distance dependent electron spin wavefunctions must overlap with certain strengths [3]. Especially silicon is a promising candidate, because it can be isotropically purified from ^{29}Si to reach an almost spin free target material. Single low energy ion implantation techniques are needed, e.g. to implant ions into the active area of FETs. Impinging ions can be detected by different effects discovered in the past, like SE emission [4, 5, 6, 7, 8], IBIC collection [9] or positive charged defects in oxides leading to an increase in the effective gate voltage [10]. In the latter case, we have previously demonstrated a current change due to the formation of positively charged defects by single antimony ions hitting the channel of an accumulation mode FET [11]. Spatial resolution can be achieved by collimating holes in the lever of an AFM, which is adjusted above the transistor and into the incident broad ion beam [6, 7, 12]. The goal is to use AFM to place single ions at precise positions.
DiVincenzo announced a list of basic requirements that a quantum computing system must satisfy in order to realize a working device, like scalability, measurability and long decoherence times [13]. Quantum algorithms like the factoring algorithm of Shore [14] have been theoretically proven and are ready to be implemented as soon as appropriate devices are available.

II. INSTRUMENTAL SETUP

The creation of Ar and Xe ions is achieved by an Electron Current Resonance (ECR) source with an extraction voltage between 0 and 12 kV, which is connected to one end of a vacuum chamber with a pressure of 10^{-6} and 10^{-8} Torr. Also attached to the chamber are Einzel lenses and quadrupole lenses for focusing the extracted ions and a 90° analyzing bending magnet to specify the desired ion species and charge state.
The ion beam hits the cantilever of a contact AFM, assembled by Persaud [15]. These cantilevers are fabricated by the group of Prof. Rangelow at the Technical University of Ilmenau, Germany, in the frame of the PRONANO Project [16]. They use a piezo-resistive Wheatstone bridge at the base of the lever for readout of the deflection signal. For static bending and dynamic excitation the cantilever is designed with materials of different expansion coefficients. By applying heat with a current through the meander shaped metallization a bimorph effect takes place. This design is very compact compared to optical readout techniques and external excitation by a piezo. It can be used in vacuum and liquid, offering high resolution imaging of biological samples in water in the latter case [17]. Crosstalk between the excitation and readout can be effectively suppressed by design or different drive techniques [18, 19, 20].
The readout signal of the cantilever is first fed into an INA110 pre-amplifier close to the cantilever to prevent noise coupling into the small bridge signal. A second pre-amplifier SR560 is connected to the first one with the possibility to balance the Wheatstone bridge signal. To prevent 60 Hz noise, the pre-amplifiers are operated by batteries. The signal is then used for the feedback system RHK SPM 1000, which controls a piezo-flexure nanopositioner of Physical Instruments with a 100 µm x 100 µm x 10 µm moving range. The sample is mounted to this stage and the cantilever is mounted on a flexure stage for coarse alignment in a 10° angle to prevent touching the sample with anything else than the tip of the cantilever. Figure 1 shows a picture of the implemented AFM setup in an eight inch vacuum cube. The ion beam pre-collimating aperture is coming from the top, which is also used to reflect the view of the sample towards a camera for coarse alignment. The cantilever is mounted to a holder below the pre-collimator, which also keeps the first pre-amplifier.

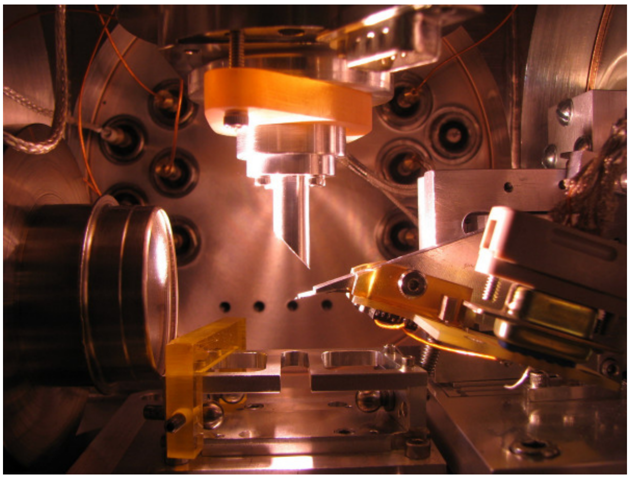

Figure 1: AFM in the vacuum chamber. One can see the pre-collimator, the cantilever holder with mounted cantilever and the preamplifier circuit.

Holes of 100 nm to 1.6 µm in the cantilever are used for implantation, which were previously drilled by a Dual Beam FIB with 30 keV Ga^{+} beam [7]. An aspect ratio of 5:1 of the thickness of the cantilever to the drilled hole size has been found. The hole is closed again by Pt deposition and a smaller hole is re-drilled into the Pt film. The Pt film must be thick enough to stop the ions used in the later implantation. The existing setup has been extended by two components, shown in red frames and arrows in Figure 2.

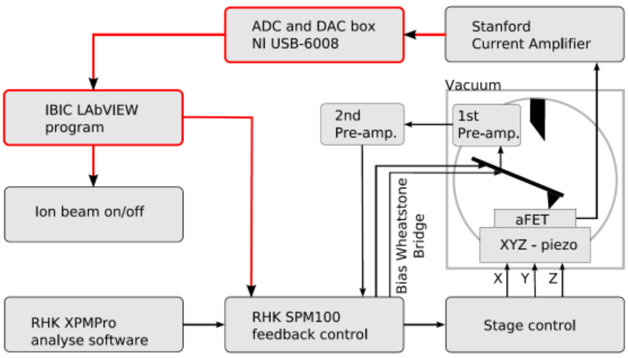

Figure 2 Experimental setup, which has been extended by the component marked in red in order to realize a closed feedback.

It represents the total feedback system for the controlled ion implantation. Software created with National Instruments (NI) LabVIEW, version 8.2, detects the ion hits in the FET channel as well as controls the SPM 1000 feedback controller and the ion beam. If a drain current change is detected through the low noise current preamplifier Stanford Research SR570 and the National Instruments USB-6008 ADC, the program will defocus the ion beam and moves the cantilever to the next position via the SPM 1000. The Stanford Research SR570 preamplifier gives a current proportional voltage as an output.

III. SOFTWARE

Figure 3 shows the user interface of the IBIC detection software.

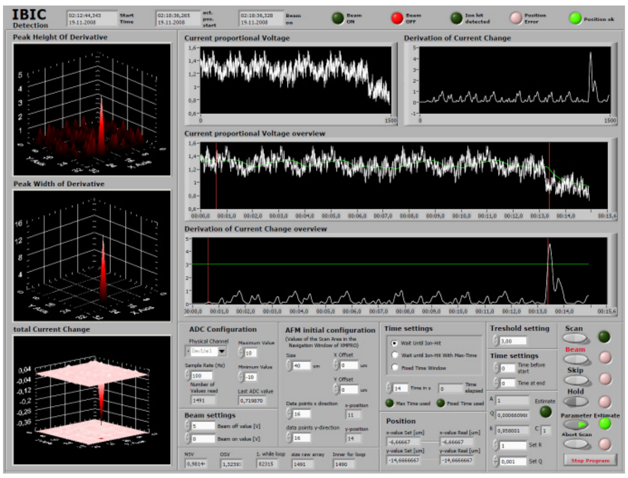

Figure 3: IBIC detection software - user interface

As mentioned before, the setup uses the external NI USB-6008 ADC to record a current proportional voltage of the drain current in the FET-channel. This device is connected via USB to the PC and offers amongst others eight 12-Bit 10 kS/s ADC. Also the feedback controller RHK SPM 1000 is connected to the same PC via Ethernet and is addressed from within LabVIEW with provided libraries from RHK [21]. The SPM 1000 receives information of the cantilever's desired position and moves it across the sample.

Values received from the ADC are first processed by a scalar Kalman filter, which observes the measured value to estimate the state of the system [22, 23, 24, 25]. The discrete calculation offers an implementation of a fast algorithm, where a past estimate is updated by a new measurement to create a present estimate. This process is divided into the Time Update, which estimates a new value and the Measurement Update, which corrects the previous estimated value of the Time Update according to the new measurement. In the case of the scalar filter, it loses its matrix form and the estimation of the Time Update is

$$\hat{x}_k^{k-1} = A\hat{x}_{k-1}^{k-1}, \qquad (1)$$

$$P_k^{k-1} = A^2 P_{k-1}^{k-1} + Q, \qquad (2)$$

where k is the time index, P is the estimation error covariance, Q is the process noise covariance, A is a state transition constant and $\hat{x}$ is the state estimate of the system. $\hat{x}_k^{k-1}$ means an estimate at time k, including information up to time k-1. The Measurement Update has the form

$$K_k = \frac{P_k^{k-1} C}{C^2 P_k^{k-1} + R}, \qquad (3)$$

$$\hat{x}_k = (1-I)y_k + I\hat{x}_k^{k-1} + K_k(y_k - C\hat{x}_k^{k-1}), \qquad (4)$$

$$P_k = P_k^{k-1}(1 - K_k C), \qquad (5)$$

where K is the Kalman gain, R is the measurement covariance, C is a measurement transition constant and y is the real measured value. Variable I can be used to further influence the estimation.

In the second consecutive step, an updated version of a Kalman Smoother is being applied. A traditional Kalman Smoother includes later measurements y^K to smooth the estimates of the state, where $K > k$ ($x_k^K = E[x_k \mid y_1, \ldots, y_K]$). Following the state estimates of the Kalman Filter, the Kalman Smoother is applied backwards, using the results of the Kalman Filter [22, 26, 27]. Therefore the Kalman Filter and Smoother have to be applied on samples, which are recorded ahead of the current sample under estimation. The large time offset and calculation time needed by this classic approach is not useful and therefore the Kalman Smoother is changed to a forward version, which calculates the smoothed values on time. The outcome of this shows a similar performance compared to the original Kalman Smoother, but with the price of a small time offset. The new equations are

$$\hat{x}_k^K = \hat{x}_k^k + J_k(\hat{x}_{k-1}^K - \hat{x}_k^k), \tag{6}$$

$$J_k = \frac{P_k^k A}{P_k^k + Q}. \tag{7}$$

An additional Moving Average Filter (MAF) can be applied consecutive to the Kalman Smoother. The MAF calculates the current state out of the past n samples. Therefore, it needs to store and calculate the sum of these n values in each iteration. Rather than doing this, the MAF can be implemented in a recursive way. The past n values and the sum of them have to be stored, too, but now each iteration consists of only one addition, one subtraction and one division.

$$y_k = \frac{y_{k-1} + x_k - x_{k-n}}{n}, \tag{8}$$

which is initialized by

$$y_n = \frac{1}{n}\sum_{i=0}^{n-1} x_{n-i}. \tag{9}$$

Variable x and y represent the input and the output of the smoother respectively. The derivative $f'(x) \approx (f(x+h) - f(x))/h$ of the signal is taken for creating peaks out of the steps. The derived values are normalized, so that noise is most likely present in the range of 0 to 1. The samples used for normalization are calculated before the measurement takes place, in the case when only noise is present. Therefore, the algorithm including the derivative is applied to a predefined amount of samples and the maximum and minimum values y_{max} and y_{min} are searched in the resulting dataset. After that, y_k can be normalized to $y_{k,n}$, where $y_{max,n}$ and $y_{min,n}$ are the maximum and minimum value to which y_k is being normalized:

$$y_{k,n} = (y_k - y_{min})\frac{y_{max,n} - y_{min,n}}{y_{max} - y_{min}} + y_{min,n} \tag{10}$$

By setting a threshold value, as indicated with a green horizontal line in the derivative chart of Figure 3, one can detect peaks originating from current changes. This allows automatic detection and following alignment to a consecutive position as well as controlling the ion beam exposure.

Often the proper values of the noise covariances R and Q of the Kalman filter are not known. They can be found by a parameter estimation, which can be used in the program. This maximum likelihood estimation maximizes a probability density function and the technique implemented is the EM algorithm [28]. In a first step a data set of AD converted values is recorded and following alternating Expectation and Maximization steps are applied to maximize the probability density function. The maximization is checked by the relative change of the current value to the previous value of the function. By falling below a threshold, the alternating steps are interrupted and the estimation is finished [29].

IV. RESULTS

Data shown in Figure 4 indicate the function of the filter and are collected in combination with a FET operated in the accumulation mode (a-FET3), which fabrication has been described elsewhere [11]. The a-FET is mounted in the vacuum chamber at room temperature, behind a pre-collimating aperture with a 1 mm hole. An aperture hole was formed in the gate of the transistor by removing the LTO layer above the channel [30]. The AFM has not been used for this experiment and the calculation is done offline afterwards. The analyzing magnet is tuned onto Xe^{6+} at an extraction voltage of 8 kV, resulting in an energy of 48 keV. The transistor is mounted on a holder, which supplies electrical contacts to the outside of the chamber. The a-FET is optically aligned to the path of the Xe beam and the beam has been defocused, so that the transistor does not show any reaction. Vertical dashed lines in the charts of Figure 4 indicate the pulses of 0.1 s each, when the ion beam is tuned onto the transistor. The transistor is biased in the linear regime with 1.1 V gate voltage and 0.1 V drain-source-voltage. The current is read out by the SR570 current amplifier and displayed and saved with a LeCroy 9354M oscilloscope (100 S/s). The current amplifier inverts ISD, resulting in a decreasing signal of the original increasing current during ion impacts. The top chart of Figure 4 shows the recorded raw data and the corresponding smoothed data, the bottom chart contains the derivative of the current.

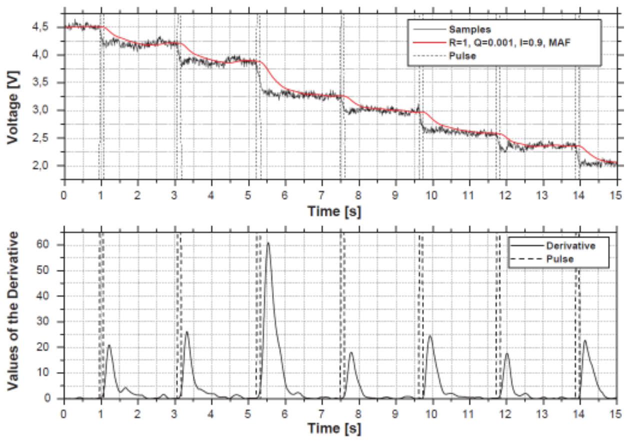

Figure 4: Several ion hits during each pulse. Vertical lines indicate the time, when the 48 keV ion beam is focused onto the a-FET3.

Figure 5 shows the effect of a lower beam current. Now each pulse of 0.1 s does not result in a step of the current anymore, as well as the steps are lower than in Figure 5. Also, the step height of every occurring current step during a pulse is in the same order of magnitude. This indicates that the remaining peaks are possibly single ion hits. In contrast, steps in Figure 4 are much higher and occur every pulse, therefore let assume several ions hitting the channel each pulse.

In the small ensemble of pulses and assumption of single ion hits in Figure 5, the probability of the amount of implanted ions per pulse can be estimated. In the condition of 3 resulting steps out of 5 pulses indicate single ion hits with a probability of ≈ 0.33 (Poisson distribution, $\lambda = 0.6$). Probability of missed hits and exactly 2 hits are ≈ 0.55 and ≈ 0.1 respectively. The beam intensities and the length of each pulse can be adjusted to statistically allow 1 hit every 10 pulses, which gives a single ion occupancy of 99 % (implantation of exactly zero or one ion, but no more than one).

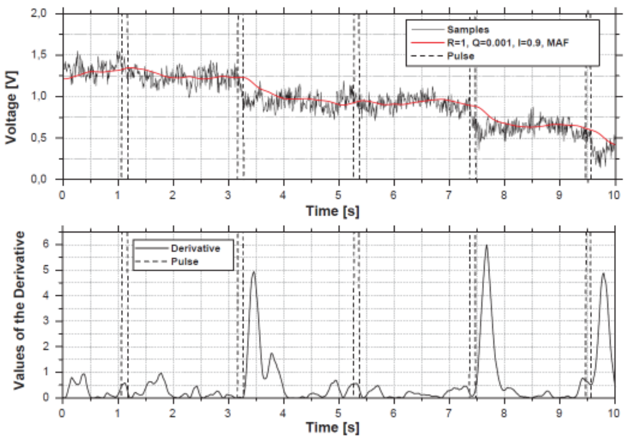

Figure 5: Single ion hits. Vertical lines indicate the time, when the 48 keV ion beam is focused onto the a-FET3.

Figure 4 and Figure 5 show a delay between ions hitting the channel and the response. This is due to the implemented filter algorithm and is hardly based on the sampling speed (around 28 ms delay at 500 Hz). It is fast enough, when the beam is tuned to statistically transmit only one ion per time interval, as mentioned before.

Maps of ion beam induced current changes have been created. This experiment was possible, since a new generation of transistors (FinFETs) have been used. The fabrication of these devices has been described elsewhere [31]. In opposite to the previous a-FETs, the active area of these FETs could be blocked by the surface of the cantilever. First, the FinFET is scanned to obtain topography information. Second, the cantilever is moved slightly away from the surface (in z-axis), so that the tip is not touching the surface anymore. No current change was observed, while the ion beam was tuned onto the transistor and the cantilever aligned to the active area. Figure 6 is a 20x20 μm^2 3-dimensional array with 21 x 21 cells, which are 1 μm apart from each other (the first cell lies on position 0 μm). The 1.6 μm diameter hole in the cantilever is used, so that an overlap between the cells in the map exists. The FinFET is biased with V_G of 1.0 V and V_D of 0.8 V. The ion species is Ar^{3+} at an extraction voltage of 12 kV (E_{kin}=36 keV) and results in a current of 450 pA on the pre-collimator. An additional 1 Hz, 12 dB low pass filter within the SR570 current amplifier is used and the sensitivity is set to 1 nA/V. The beam dwell time is 5 s and the sampling rate is 200 S/s. On average, 600 ion/s/µm^2 hit the sample [31]. The noise results in current changes of positive and negative values, which are overlaid by the effect of ion impacts. But only absolute values of these changes are considered here. The highest peak is located at a change of 13.25 nA and the noise is present between 0 and 2.6 nA.

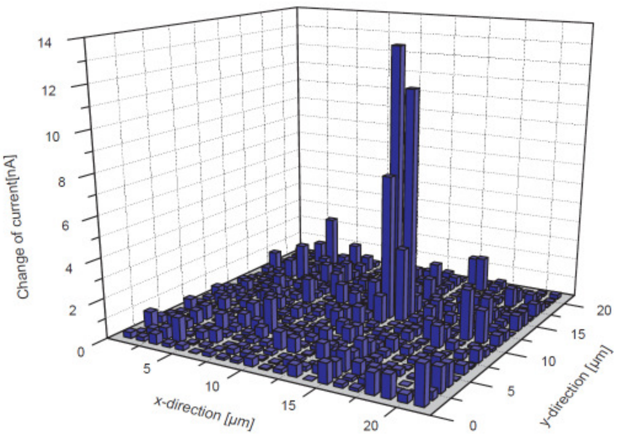

Figure 6: Array of 21 x 21 cells, each 1 µm and collimated by a 1.6 µm diameter hole.

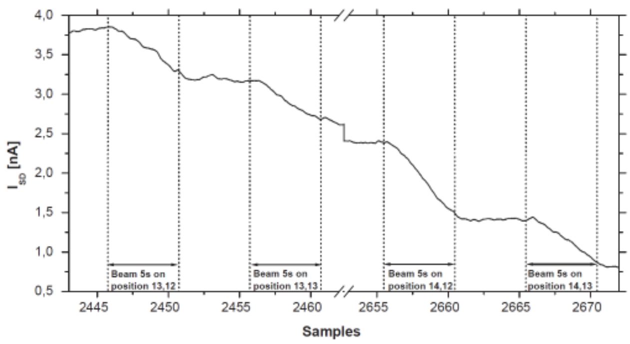

Figure 7: Change of I_{SD} during ion beam exposure. Vertical lines indicate the time, when the ion beam is tuned onto the transistor.

The four highest current changes of ISD in Figure 6 during the ion beam exposures are shown in Figure 7, where every two cells are scanned back-to-back. The beam dwell times as well as the positions within the array are indicated.

Figure 8 is a 3 x 3 µm2 array with 16 x 16 cells, where a hole of 100 nm diameter in the cantilever is used. The spots are separated by 200 nm. The FinFET is biased with V_G of 1.0 V and V_D of 0.8 V. The ion species is Ar^{2+} at an extraction voltage of 10 kV (E_{kin}=20 keV). A 1 Hz low pass filter in the current amplifier is used and the sensitivity is set to 1 nA/V.

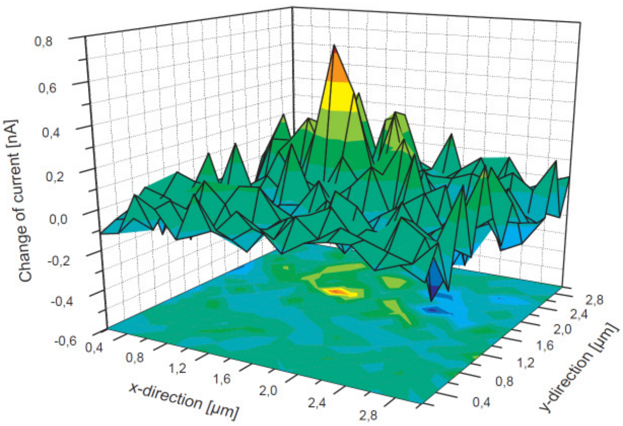

Figure 8: 3-dimensional array of 16 x 16 cells, each 200 nm and collimated by a 100 nm diameter hole.

The time the ion beam is focused onto the FinFET is 30 s and the sampling rate is 300 S/s. The signs of all samples have been inverted again by the current amplifier. The peak is formed by around 2 values, where the highest one is 0.7 nA. The surrounding noise has values between -0.55 nA and 0.39 nA. On average, approx. 1500 ion/s/µm^2 hit the sample [31].

V. DISCUSSION AND OUTLOOK

Since precise placement of single donors in solid states requires a new kind of ion implantation, the impinging ions must be detected and controlled one by one. The loop between the ion beam induced variation of the transistor channel current and control of the collimating AFM setup must be closed. The present work addressed this by extending the existing setup with the LabVIEW based software, which controls the AFM feedback controller based on the information derived from the transistor channel current. The implemented filter algorithm was able to detect ion hits out of noisy measurements. The response time, until the ion beam can be defocused due to detected ion hits, is hardly based on the sampling speed. In this case, it depends on how fast the samples can be processed by the software, which is lower than the maximum sampling rate of the ADC in this implementation. Execution speed of the LabVIEW based software can be sped up by code optimization, compiling the code or implementation in a different language. The IBIC detection algorithm has been successfully tested in combination with current changes in the a-FET3 during ion beam exposures. By being able to block the active area of the new FinFETs with the cantilever, compared to the predecessors, the mapping of arrays due to ion beam induced current changes could be done. Although it was impossible to show single ion hits in the maps, automatic alignment of the AFM cantilever in respect to the transistor and control of the ion beam could be successfully demonstrated. As soon as the FinFETs are able to react to single ions like the predecessor, arrays of single ions can be addressed to implant.

VI. ACKNOWLEDGEMENTS

Funding of the cantilever work was provided by the European Commission in the frame of the 6th Program PRONANO-"Technology for the Production of Massively Parallel Intelligent Cantilever Probe Platforms for Nanoscale Analysis and Synthesis", Contract No. IP 515739.

We thank the staff of the Microlab at UC Berkeley and the staff of the Molecular Foundry and the National Center for Electron Microscopy at LBNL for their support. This work was supported by NSA under contract number MOD 713106A, the National Science Foundation through NIRT Grant No. CCF-0404208, and by the Director, Office of Science, of the Department of Energy under Contract No. DE-AC02-05CH11231.

VII. REFERENCES

[1] T. Shinada, S. Okamoto, T. Kobayashi, and I. Ohdomari, "Enhancing semiconductor device performance using ordered dopant arrays," Nature 437, pp. 1128–1131 2005.

[2] T. Shinada, A. Ishikawa, C. Hinoshita, M. Koh, and I. Ohdomari, "Reduction of fluctuation in semiconductor conductivity by one-by-one ion implantation of dopant atoms," Nanotechnology 19:345202 2000.

[3] B. E. Kane, "A silicon-based nuclear spin quantum computer," Nature 393, pp. 133–137, 1998.

[4] T. Shinada, A. Ishikawa, M. Fujita, K. Yamashita, and I. Ohdomari, "Influence of secondary electron detection effiency on controllabilityof dopant ion number in single ion implantation," Nature 393, pp. 133–137, 1998.

[5] T. Schenkel, J. Meijer, A. Persaud, J. W. McDonald, J. P. Holder, and D. H. Schneider, "Single ion implantation for solid state quantum computer development," Proceedings of SPIE Quantum Dot Devices and Computing 4656:0201549, 2002.

[6] A. Persaud, F. I. Allen, F. Gicquel, S. J. Park, J. A. Liddle, T. Schenkel, T. Ivanov, K. Ivanova, I. W. Rangelow, and J. Bokor, "Single ion implantation with scanning probe alignment," American Vacuum Society B 22 (6), pp. 2992–2993, 2004.

[7] A. Persaud, S. J. Park, J. A. Liddle, T. Schenkel, J. Bokor, and I.W. Rangelow, "Integration of scanning probes and ion beams," Nanoletters 5 (6), pp. 1087–1091, 2005.

[8] T. Shinada, T. Kurosawa, H. Nakayama, Y. Zhu, M. Hori, and I. Ohdomari, "A reliable method for the counting and control of single ions for single-dopant controlled devices," Nanotechnology 19:345202, 2008.

[9] D. N. Jamieson, C. Yang, T. Hopf, S. M. Hearne, C. I. Pakes, S. Prawer, M. Mitic, E. Gauja, S. E. Andresen, F. E. Hudson, A. S. Dzurak, and R. G. Clark, "Controlled shallow single ion implantation in silicon using an active substrate for sub-20-kev ions," Applied Physics Letters 86:202101, 2002.

[10] T. A. Ma, Paul V. Dressendorfer, "Ionizing Radiation Effects in MOS Devices & Circuits", Wiley, New York, 1989

[11] A. Batra, C. D. Weis, J. Reijonen, A. Persaud, T. Schenkel, S. Cabrini, C. C.lo, and J. Bokor, "Detection of low energy single ion impacts inmicron scale transistors at room temperatur," Applied Physics Letters 91, pp. 91–93, 2007.

[12] J. Meijer, S. Pezzagna, T. Vogel, B. Burchard, H. H. Bukow, I. W. Rangelow, Y. Sarov, H. Wiggers, I. Plmel, F. Jelezko, J. Wrachtrup, F. Schmidt-Kaler, W. Schnitzler, and K. Singer, "Towards the implanting of ions and positioning of nanoparticles with nm spatial resolution," Applied Physics A 91, pp. 567–571, 2008.

[13] D. P. DiVincenzo, "The physical implementation of quantum computation," Quantum Physics arXiv:quantph/0002077v3, IBM, 1992.

[14] Peter W. Shor, "Polynomial-time algorithms for prime factorization and discrete logarithms on a quantum computer," SIAM J. Comput. 26, pp. 1484–1509, 1997, ISSN 0097-5397.

[15] Arun Persaud, "Aligned Ion Implantation using Scanning Probes", PhD dissertation, Johann Wolfgang Goethe-Universitaet, Frankfurt am Main and Berkeley, Germany and California, December 2006.

[16] I.W. Rangelow, "Scanning proximity probes for nanoscience and nanofabrication" Microelectronic Engineering, Volume 83 (4-9), pp. 1449-1455, April-September 2006

[17] G.E. Fantner, W. Schumann, R.J. Barbero, A. Deutschinger, V. Todorov, D.S. Gray, A.M. Belcher, I.W. Rangelow and K.Youcef-Toumi, "Use of actuating and self sensing cantilevers for imaging biological samples in liquid", Nanotechnology, 2009

[18] A.Frank, J.-P. Zöllner, Y. Sarov, Tz. Ivanov, St. Klett, T. Gotszalk, M. Zielony, P. Zawierucha, B. Schmidt, M. Zier, M. Nikolov, W. Engl, T. Sulzbach, D. Dontsov, E. Langlotz, W. Schott and I.W. Rangelow, "Investigation of Crosstalk in Cantilever Arrays", Proceedings Eurosensors / XXII, Dresden, Germany, pp. 744-747, 2008

[19] R. Pedrak, Tzv. Ivanov, T. Gotszalk, P. Hudek, O. Fortagne and I. W. Rangelow, "Micromachined AFM sensor with integrated piezoresistive sensor and thermal bimorph actuator for high-speed tapping-mode AFM and phase-imaging in higher eigenmodes" J. Vav. Sci. Technology, B 21N60, pp. 3102-3107 2003.

[20] Georg E. Fantner, Daniel J. Burns, Angela M. Belcher, Ivo W. Rangelow, and Kamal Youcef-Toumi, "DMCMN: In Depth Characterization and Control of AFM Cantilevers With Integrated Sensing and Actuation", J. Dyn. Sys., Meas., Control 131, 061104, 2009, DOI:10.1115/1.4000378

[21] RHK-Technology. Imaging the Future of Nanoscience. http://www.rhk-tech.com/.

[22] A. V. Balakrishnan, "Kalman Filtering Theory" , Optimization Software, Inc., Publications Division, New York, 1984, ISBN 978-0911575262.

[23] Dan Simon, "Kalman filtering," Embedded Systems Programming 14(6), pp. 72–79, 2001.

[24] G.Welch and G. Bishop, "An Introduction to the Kalman Filter", Department of Computer Science, University of North Carolina at Chapel Hill, NC, 2006.

[25] P. S. Maybeck, Stochastic Models, "Estimation and Control Volume 1", Academic Press, 1979.

[26] M.Welling, "The Kalman Filter", California Institute of Technology Pasadena http://www.stat.columbia.edu/~liam/teaching/neurostat-spr07/papers/hmm/KF-welling-notes.pdf.

[27] S. Särkkä, A. Vehtari, and J. Lampinen, "Time series prediction by Kalman smoother with cross-validated noise density," In Proceedings of the International Joint Conference on Neural Networks, pp. 1615–1619, 2004.

[28] G. J. McLachlan and T. Krishnan, "The EM Algorithm and Extensions", 1st ed., Wiley-Interscience, 1996, ISBN 978-0471123583.

[29] M. E. Khan and D. N. Dutt. "An Expectation-Maximization Algorithm Based Kalman Smoother Approach for Event-Related Desynchronization (ERD) Estimation from EEG". IEEE Transactions on Biomedical Engineering, 54(7), pp. 1191-1198, 2007.

[30] C. D.Weis, A. Schuh, A. Batra, A. Persaud, I.W. Rangelow, J. Bokor, C. C. Lo, S. Cabrini, E. Sideras-Haddad, G. D. Fuchs, R. Hanson, D. D. Awschalom, and T. Schenkel, "Single-atom doping for quantum device development in diamond and silicon," Journal of Vacuum Science and Technology B 26(6), pp. 2596–2600, 2008.

[31] Weis CD, Schuh A, Batra A, Persaud A, Rangelow IW, Bokor J, Lo CC, Cabrini S, Olynick D, Duhey S, Schenkel T, "Mapping of ion beam induced current changes in FinFETs" Nuclear Instruments & Methods In Physics Research Section B, 267, 8-9, pp. 1222-1225, 2009